Localization of optical vortices in nonlinear hexagonal multicore fibers

Shamaem Khushhali [●],[1,][*] Raju Adhikary,[2] Carino Ferrante,[3] Cristian Antonelli,[2]
Antonio Mecozzi [●],[2] Andrea Marini [●],[2,3,][†] and Samudra Roy [●][1,][‡]

[1]*Department of Physics, Indian Institute of Technology Kharagpur, West Bengal 721302, India*
[2]*Department of Physical and Chemical Sciences, University of L'Aquila, Via Vetoio, 67100 L'Aquila, Italy*
[3]*CNR-SPIN, c/o Dipartimento di Scienze Fisiche e Chimiche, University of L'Aquila, Via Vetoio, Coppito 67100 L'Aquila, Italy*

We investigate the existence and stability of vortexlike collective excitations in nonlinear (NL) multicore fibers (MCFs). We focus on realistic cored and coreless hexagonal MCFs where every core operates in the single-mode regime while displaying polarization degeneracy. We model the propagation dynamics of vortex fields in such MCF structures by NL discrete Schrödinger equations, finding families of homogeneouslike NL vortex fields with constant power distribution over peripheral cores. By analyzing the stability of such collective modes with distinct topological charges against perturbations, we find that they are all unstable. We further investigate the existence and stability of inhomogeneous NL vortex fields, finding only one stable nonspinning localized NL mode with vanishing topological charge in a narrow power range only for cored hexagonal MCFs. Our results are relevant for the manipulation and control of collective excitations in NL MCFs, indicating that self-organization into stable localized collective modes can be exploited in innovative MCF-based communication systems.

I. INTRODUCTION

Optical vortices (OVs) hold significant potential for a wide range of applications, e.g., high-capacity optical communications [1,2], microscopy [3,4], and information transmission [5]. Optical-vortex-based traps are routinely used in biology and medicine for the micromanipulation of living cells [6] and chromosomes [7]. Moreover, OVs enable micromachine management without external mechanical contact in a sealed environment [8]. In addition, due to their intensity and phase features, OVs are promising for applications in optical switching, modulation, and sensing. Indeed, they possess an intrinsic phase vorticity characterized by an integer winding number [9], also called topological charge (TC), that can be adopted, e.g., for spatial-division multiplexing. Because the OV wave front encompasses a screwlike motion determined by the TC, its propagation results in circular energy flow accompanied by orbital angular momentum (OAM) [10–14].

In nonlinear (NL) media, the balance between diffraction and self-focusing nonlinearity can lead to the formation of localized self-sustaining waves, known as spatial solitons. Solitons with embedded OAM, also named vortex solitons [9], are not stable in homogeneous NL media owing to azimuthal instability produced by focusing nonlinearity [15,16]. Diverse mechanisms, e.g., NL potentials [17], nonlocality [18,19], and two-photon absorption [20], can be employed to hamper azimuthal instability. Moreover, twisted waveguide arrays with discrete rotational symmetry [21] and two-dimensional optically induced photonic lattices [22,23] support stable discrete vortex soliton formation.

Multicore fibers (MCFs), consisting of multiple cores embedded within the same cladding, can support vortex fields, particularly promising for spatial-division multiplexing in high-capacity fiber-optic communication systems [24–27]. The interplay between NL optical dynamics and phase vorticity can be accounted by the discrete NL Schrödinger equation (DNLSE) in the weak-coupling approximation [2]. Moreover, the DNLSE enables one to account for nonlinearity-induced thermalization [28–30], wave condensation and turbulence [31–33], spatiotemporal pulse compression [34,35], and beam self-cleaning [36–38] in multimode fibers.

Here we investigate theoretically the existence, stability, and localization properties of discrete OVs (DOVs) in cored and coreless hexagonal MCFs operating in the single-mode regime and with polarization degeneracy. By assuming weak Kerr nonlinearity and coupling between the fiber cores, we model optical propagation by DNLSEs, finding diverse families of homogeneouslike NL DOVs with distinct TCs and uniform power distribution over peripheral cores. By analyzing the stability of such NL DOVs over propagation, we find that they are unstable. Such a stability scenario hints at the possible existence of localized NL modes with nonuniform power distribution over peripheral cores, which we investigate systematically by a Newton-Raphson algorithm finding diverse inhomogeneous NL DOV families. Finally, we investigate the stability of such NL DOVs under perturbation, finding that only NL DOVs with vanishing TC can be stable in cored hexagonal MCFs within a narrow power range. Our results are relevant for NL self-cleaning applications in MCFs.

II. MODEL

We focus on (a) coreless and (b) cored hexagonal MCFs composed of (a) $N = 6$ peripheral cores and (b) a central

[*]Contact author: shamaemkhushhali@kgpian.iitkgp.ac.in
[†]Contact author: andrea.marini@univaq.it
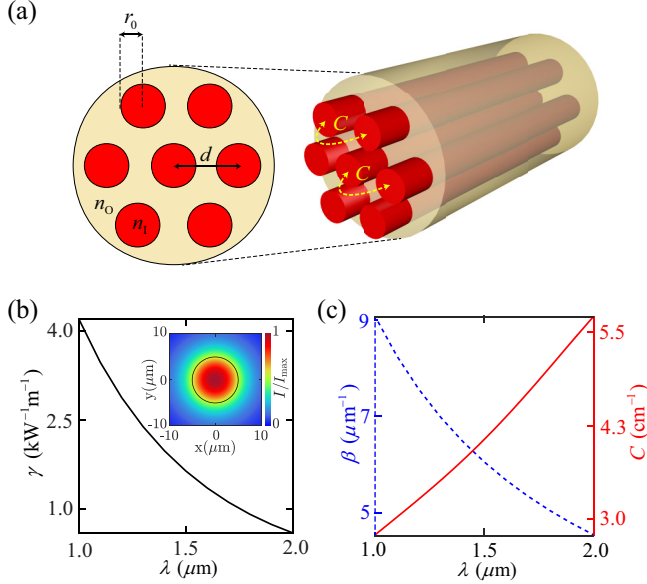[‡]Contact author: samudra.roy@phy.iitkgp.ac.in

(a)

(b)

(c)

FIG. 1. (a) Setup of the considered MCFs composed of $N = 6$ (coreless) peripheral cores and a (cored) central core. Every core has a doped silica base and a radius $r_0 = 5$ μm, and the intercore distance is assumed to be $d = 15$ μm. The core ($n_I = 1.4446$) and cladding (silica with different doping concentration $n_O = 1.4420$) refractive indices are approximated to their value at wavelength $\lambda = 1.5$ μm. (b) Dependence of the effective NL coefficient $\gamma(\lambda)$ as a function of the vacuum wavelength λ for the HE_{11} mode of every core. The inset shows the intensity spatial profile. (c) Wavelength dependence of the core propagation constant $\beta(\lambda)$ (blue dashed curve) and coupling coefficient $C(\lambda)$ (red solid curve).

core with radii $r_0 = 5$ μm and intercore distance $d = 15$ μm [see Fig. 1(a)]. We assume realistic hexagonal MCFs where every core is composed of germanium-doped silica (with refractive index $n_I = 1.4446$ at $\lambda = 1.5$ μm), while the cladding is based on the same material with distinct germanium doping (with refractive index $n_O = 1.4420$ at $\lambda = 1.5$ μm). Our main results below refer to $\lambda = 1.5$ μm and we highlight that dispersion of germanium-doped silica should be taken into account to attain consistent results for different operating wavelengths. We emphasize that in typical hexagonal MCFs currently adopted for optical communications, the intercore distance d is larger in order to attain weak coupling and hamper nonlinear effects by coupling noise. However, because we aim at investigating collective NL dynamics in the considered MCFs, we focus here on a realistic configuration where coupling is higher (equivalent to a centimeter length scale) and we can safely neglect coupling noise. Moreover, we focus on ultrafast excitation with greater than 10 ps duration such that dispersion is negligible and we can model optical propagation in the slowly varying envelope approximation neglecting group-velocity dispersion [39–41]. Owing to the small refractive-index variation between core and cladding media $\Delta n = n_I - n_O$, every MCF core behaves like a weakly guiding step-index optical fiber [42] supporting only one mode (with polarization degeneracy), which couples with the other cores' modes. Indeed, at the considered wavelength $\lambda = 1.5$ μm, every core supports only one HE_{11} mode [see

the inset in Fig. 1(b)], with linear propagation constant $\beta = 6.051$ μm^{-1} and polarization degeneracy. Collective excitations in the considered systems arise from intersite linear coupling and on-site Kerr nonlinearity, which can be modeled by DNLSEs for the optical field with amplitudes $\phi_w^{(j)}$ (here $j = 1, 2$ labels the two distinct polarizations of light in every core) at the core sites labeled by the index w ($w = 0$ indicates the central core, while $w = 1, \ldots, N$ indicates the peripheral cores). Note that, owing to the periodicity of the considered system, the peripheral core amplitudes satisfy periodic boundary conditions (BCs) $\phi_w^{(j)} = \phi_{w+6}^{(j)}$ (for $w > 0$ since we label the core by $w = 0$). Explicitly, DNLSEs for the considered systems are given by

$$i\partial_z \psi_w^{(j)} + C(\psi_{w+1}^{(j)} + \psi_{w-1}^{(j)} + \psi_0^{(j)})$$
$$+ \gamma(|\psi_w^{(j)}|^2 + 2|\psi_w^{(3-j)}|^2)\psi_w^{(j)} = 0, \quad (1)$$

$$i\partial_z \psi_0^{(j)} + C\sum_{w=1}^{N} \psi_w^{(j)} + \gamma(|\psi_0^{(j)}|^2 + 2|\psi_0^{(3-j)}|^2)\psi_0^{(j)} = 0, \quad (2)$$

where $\psi_w^{(j)} = \phi_w^{(j)} e^{-i\beta z}$ is the rescaled field amplitude and z is the longitudinal propagation direction of the considered MCFs. Note that, owing to the cylindrical symmetry of the MCF cores, linear intercore cross-polarization couplings vanish, while self-polarization couplings are degenerate [43] with coefficients $C = 4.11$ cm^{-1} and explicitly given by

$$C = \frac{q_O K_0(q_O k_0 d)}{n_I k_0 r_0^2 (q_O^2 - q_I^2) K_1^2(q_O k_0 r_0)}, \quad (3)$$

where $q_{O,I} = \sqrt{(\beta/k_0)^2 - n_{O,I}^2}$, $k_0 = 2\pi/\lambda$, and K_n is the nth-order modified Bessel function of the first kind. On-site Kerr nonlinearity is accounted for by an effective NL parameter accounting also for surface nonlinearity contributions [44], explicitly given by

$$\gamma = 2\pi n_2 (k_0/\beta)^2 \frac{\int_0^\infty \rho n^2(\rho)[2|e(\rho)|^4 + |e^2(\rho)|^2]d\rho}{\int_0^\infty \rho \, \mathrm{Re}[e(\rho) \times h^*(\rho)] \cdot \hat{e}_z d\rho}, \quad (4)$$

where $\rho = |\mathbf{r} - z\hat{e}_z|$, with $\mathbf{r} = x\hat{e}_x + y\hat{e}_y + z\hat{e}_z$ the position vector with components $x = \mathbf{r} \cdot \hat{e}_x$, $y = \mathbf{r} \cdot \hat{e}_y$, and $z = \mathbf{r} \cdot \hat{e}_z$ with respect to the unit vectors $\hat{e}_{x,y,z}$; $n^2(\rho) = n_I^2 \Theta(r_0 - \rho) + n_O^2 \Theta(\rho - r_0)$, with $\Theta(x)$ the Heaviside step function; $n_2 = 2.7 \times 10^{-20}$ W/m^2 is the Kerr coefficient of silica; and $\mathbf{e}(\rho)$ and $\mathbf{h}(\rho)$ are the electric- and magnetic-field complex vector profiles of the considered HE_{11} modes, respectively, which we do not report here for the sake of brevity. At the considered wavelength $\lambda = 1.5$ μm we calculate numerically the integral above, obtaining $\gamma = 1.6$ kW^{-1} m^{-1}. The dimensionless parameters 1 and 2 in front of $|\psi_{w,0}^{(j)}|^2$ and $|\psi_{w,0}^{(3-j)}|^2$ indicate the distinct self-polarization and cross-polarization NL contributions, respectively. The wavelength dependences of the NL parameter γ, core propagation constant β, and intercore coupling coefficient C are illustrated in Figs. 1(b) and 1(c). We emphasize that our approach applies to MCFs with cores supporting single-mode propagation, while multimode dynamics requires more sophisticated approaches beyond the DNLSE to account for noise-induced random coupling within groups of degenerate modes, e.g., Manakov equations [45].
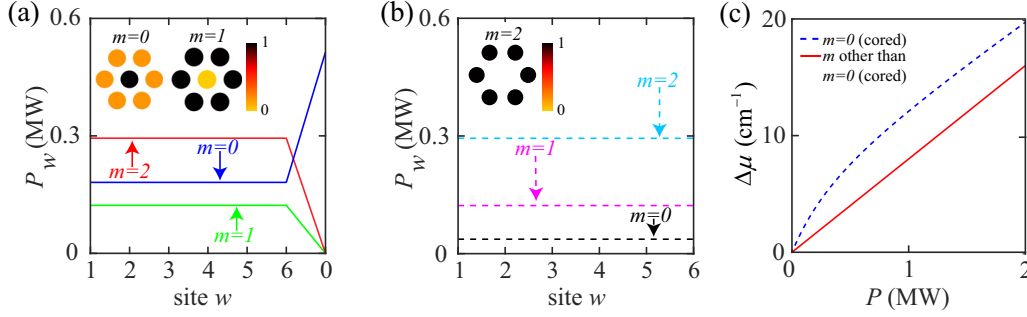
FIG. 2. Homogeneouslike NL mode profiles of the considered (a) cored (solid lines) and (b) coreless hexagonal MCFs (see Fig. 1) for TCs $m = 0, 1, 2$ and fixed NL propagation constant $\mu = 6.052$ μm^{-1}. The inset shows the polarization-independent transverse power distribution P_w of cored and coreless MCFs. (c) NL dispersion depicting the dependence of the total power P as a function of the propagation constant correction $\Delta\mu = \mu - \mu_1$ for $m = 0$ and $m \neq 0$. Note that, while for $m = 0$ the NL dispersions of cored and coreless MCFs are distinct, they coincide for $m \neq 0$ due to the vanishing field amplitude at the central core.

III. DISCRETE OPTICAL VORTICES

A. Homogeneouslike NL modes

Homogeneouslike NL modes of Eqs. (1) and (2) are found in the form of stationary DOVs with the TC m satisfying the periodic BCs $\psi_w^{(j)} = \psi_{w+6}^{(j)}$ (for $w > 0$) by taking the ansatz

$$\psi_w^{(j)} = \Psi^{(j)} e^{i(\mu z + h w)}, \tag{5a}$$

$$\psi_0^{(j)} = \delta_{m,0} \Psi_0^{(j)} e^{i(\mu z + h w)}, \tag{5b}$$

where $\delta_{m,0}$ indicates the Kronecker delta function, $\Psi^{(j)}$ and $\Psi_0^{(j)}$ indicate the complex amplitudes of the j polarization peripheral and central core fields, respectively, μ is the NL propagation constant of the considered DOVs, and $h = 2\pi m / N$. Note that, due to the vanishing cross-polarization linear coupling and the global phase invariance of DNLSEs, the relative phase between the two distinct polarization amplitudes is arbitrary. Inserting the above ansatz in Eqs. (1) and (2), we get a system of four complex algebraic equations for the complex amplitudes $\Psi^{(1,2)}$ and $\Psi_0^{(1,2)}$, which we solve numerically by a Newton-Raphson algorithm enabling the calculation of such complex amplitudes for every NL propagation constant μ and TC m. In Figs. 2(a) and 2(b) we illustrate the polarization-independent power distributions $P_w = P_w^{(1,2)} = |\psi_w^{(1,2)}|^2$ of the considered homogeneouslike NL DOVs for (a) cored and (b) coreless MCFs with distinct TCs m and NL propagation constant μ. For such NL DOVs, we further illustrate the dependence of the NL propagation constant correction $\Delta\mu = \mu - \mu_1$ over the total power in Fig. 2(c), where $\mu_1 = 2C \cos h$ is the linear propagation constant (for $\gamma = 0$). Note that, while $m \neq 0$ modes (coinciding for both cored and coreless hexagonal MCFs due to the vanishing field amplitude at the core) display the common linear $\Delta\mu$ vs total power $P = \sum_w P_w$ dependence, the NL dispersion relation of $m = 0$ modes is more involved due to the coupling with the central core. Indeed, owing to the hexagonal structure, the central core is coupled to *all* the peripheral cores, which conversely are coupled only to their nearest neighbors. Such a distributed coupling of the central core to all peripheral cores produces a NL $\Delta\mu$ vs P dependence for $m = 0$ NL DOVs (in cored MCFs). Moreover, such localized NL DOVs present a localized peak at the MCF core

[see Fig. 2(a)] on top of a uniform peripheral background, similarly to gray solitons.

B. Stability of homogeneouslike NL DOVs

In principle, the stability of homogeneouslike NL DOVs may be investigated by the system Hamiltonian minima. However, in order to gain insight into the instability perturbations and corroborate our numerical findings, we take the ansatz

$$\psi_w^{(j)} = (\Psi^{(j)} + \delta\Psi_+^{(j)} e^{gz + ilw} + \delta\Psi_-^{j*} e^{g^*z - ilw}) e^{i(\mu z + hw)}, \tag{6a}$$

$$\psi_0^{(j)} = \delta_{m,0} (\Psi_0^{(j)} + \delta\Psi_{0+}^{(j)} e^{gz} + \delta\Psi_{0-}^{j*} e^{g^*z}) e^{i\mu z}, \tag{6b}$$

where l is the arbitrary winding number of the perturbation field and g is a complex coefficient whose real part Re(g) indicates the longitudinal growth rate of small perturbations with amplitudes $\delta\Psi_\pm^{(j)}$ and $\delta\Psi_{0\pm}^{(j)}$. Inserting in Eqs. (1) and (2) the ansatz above, with the assumptions $|\delta\Psi_\pm^{(j)}| \ll |\Psi_\pm^{(j)}|$ and $|\delta\Psi_{0\pm}^{(j)}| \ll |\Psi_\pm^{(j)}|$, we get the linearized homogeneous system of equations $\hat{\mathbf{M}}_H \delta\boldsymbol{\Psi} = 0$, where $\delta\boldsymbol{\Psi}$ is an eight-component array containing the amplitude perturbations $\delta\Psi_\pm^{(j)}$ and $\delta\Psi_{0\pm}^{(j)}$, and $\hat{\mathbf{M}}_H$ is a cumbersome 8×8 coefficient matrix that we do not report here for the sake of brevity. Nontrivial solutions are obtained by setting a vanishing discriminant det$\hat{\mathbf{M}}_H = 0$, leading to a complex NL algebraic equation for the growth rate g. We solve numerically such an equation by a Newton-Raphson algorithm, enabling us to calculate the gain spectrum Re[$g(l)$] for every homogeneouslike NL DOV mode with total power P, TC m, and every fixed perturbation TC l.

In Fig. 3(a) we plot the instability gain parameter Re(g) as a function of the total power P for the considered cored (solid line) and coreless (dashed line) hexagonal MCFs. Note that, because the gain parameter is positive [Re(g) > 0], all the considered extended DOVs are unstable since small-amplitude perturbations are amplified over propagation. We further confirm such calculations by the direct numerical solution of Eqs. (1) and (2) by a fourth-order Runge-Kutta algorithm provided with a perturbed NL DOV at the input. In Figs. 3(b) and 3(c) we plot the results of such numerical simulations for the considered cored and coreless hexagonal
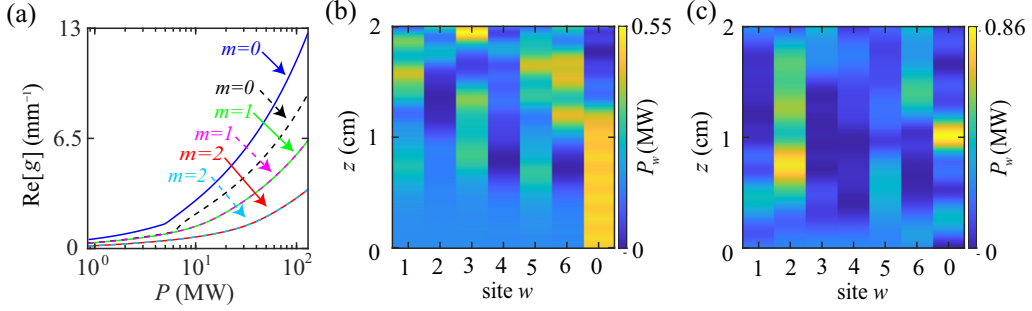
FIG. 3. (a) Linear stability analysis spectrum illustrating the dependence of the maximum instability eigenvalue [accounted for by the real part of the complex gain eigenvalue Re(g)] as a function of the MCF total power P and distinct TCs $m = 0, 1, 2$. Also shown is the propagation dynamics of homogeneouslike NL modes of the cored MCF perturbed by random fluctuations for fixed $P = 1.5$ MW and (b) $m = 0$ and (c) $m = 1$.

MCFs, respectively, confirming the stability scenario provided by linear stability analysis.

C. Inhomogeneous NL DOVs

The stability scenario described above indicates the existence of other localized NL DOVs with inhomogeneous power distribution over the peripheral cores, similarly to discrete solitons in extended waveguide arrays [46–48]. In order to investigate systematically the existence of such inhomogeneous collective excitations, we take the ansatz

$$\psi_w^{(j)} = \Psi^{(j)}(w)e^{i\mu z + ihw}, \tag{7a}$$

$$\psi_0^{(j)} = \delta_{m,0}\Psi_0^{(j)}e^{i\mu z + ihw}, \tag{7b}$$

where the peripheral core amplitudes $\Psi^{(j)}(w)$ are not uniform but are dependent on the site w. Inserting the ansatz above in Eqs. (1) and (2), one gets a system of 14 coupled NL equations, which we solve numerically by a Newton-Raphson algorithm for every propagation constant μ. We find several families of inhomogeneous NL DOVs with distinct TCs m. In Figs. 4(a) and 4(b) we illustrate their power distributions for distinct TCs $m = 0, 1, 2$ and fixed propagation constant $\mu = 6.052 \ \mu m^{-1}$ and fixed power $P = 1$ MW, respectively, while in Fig. 4(c) we plot their NL dispersion relations $\Delta\mu = \mu - \beta_1$ vs total power P. Again, we emphasize that the reported $m = 0$ NL DOVs refer to cored hexagonal MCFs (and do not exist for coreless MCFs), while $m \neq 0$ NL DOVs coincide for both cored and coreless MCFs owing to the vanishing field amplitude at the core. Note that $m = 1, 2$ NL DOVs are peaked at two opposite peripheral cores and have lower value at the other cores for the total power $P = 1$ MW. In turn, owing to the doubled-peak nature of such NL localized modes, they are of higher order with respect to the $m = 0$ (cored MCF) homogeneouslike NL DOVs presenting a power peak at the central core embedded within a lower homogeneous power background [see Fig. 2(a)]. For comparison, in Fig. 4(d) we plot the NL dispersion relations $\Delta\mu$ vs P for the $m = 0$ ① homogeneouslike and ② inhomogeneous NL DOVs, illustrated in Fig. 4(e) for $P = 1.5$ MW. Note that, as discussed above, inhomogeneous solutions are of higher order and exist above a critical power threshold where they bifurcate from homogeneouslike solutions.

D. Stability of inhomogeneous NL DOVs

In order to investigate the stability of inhomogeneous NL DOVs, we take the ansatz of Eqs. (5a) and (5b) with the prescription that the peripheral core amplitudes $\Psi^{(j)}(w)$ depend over the site w. Inserting the ansatz into Eqs. (1) and (2), we linearize the ensuing 28×28 algebraic system of equations to
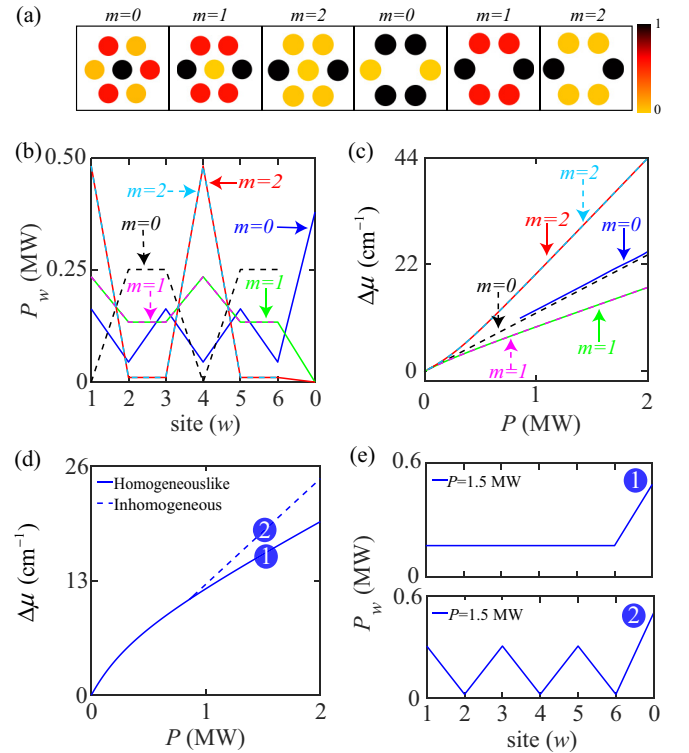

FIG. 4. (a) Power distribution of inhomogeneous NL DOVs over the distinct cores for TCs $m = 0, 1, 2$, for both the cored and coreless MCFs considered. (b) Inhomogeneous NL DOV profiles of cored (solid lines) and coreless (dashed lines) MCFs for TCs $m = 0, 1, 2$ and fixed total power $P = 1$ MW. (c) NL dispersion relation $\Delta\mu$ vs P of cored (solid lines) and coreless (dashed lines) MCFs for different TCs. (d) NL dispersion relation of $m = 0$ ① homogeneouslike and ② inhomogeneous NL DOVs for cored MCFs. (e) Field profiles of ① homogeneouslike and ② inhomogeneous NL DOVs for $P = 1.5$ MW.
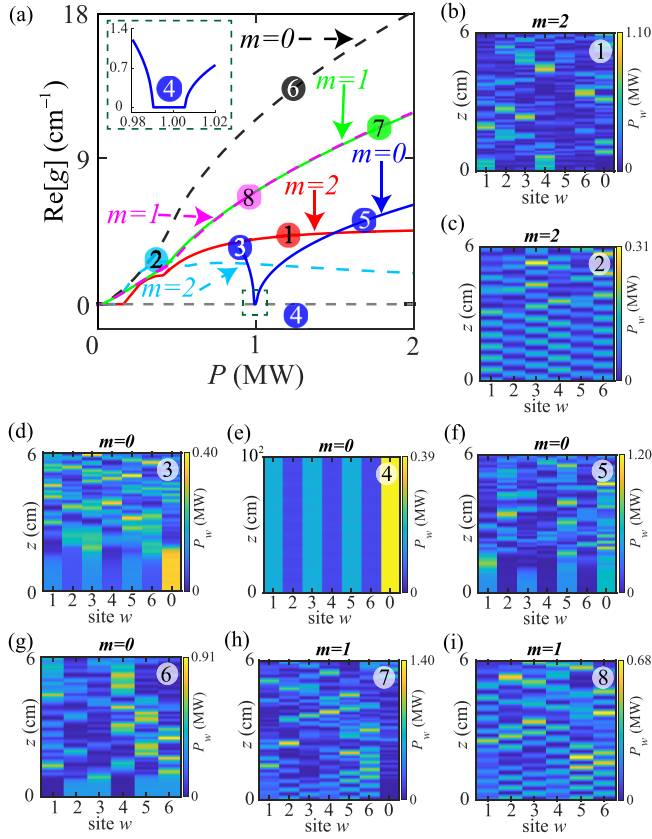
FIG. 5. (a) Gain spectrum of inhomogeneous NL DOVs, where the instability gain parameter Re(g) is plotted vs the total power P of NL DOVs with distinct TCs $m = 0, 1, 2$ for fixed $l = 2\pi/6$. (b)–(f) Propagation of randomly perturbed NL DOVs for TCs $m = 0, 1, 2$ with distinct total power labeled ①–⑧ in (a). The inset in (a) shows a narrow stability window observed for $m = 0$ (cored MCFs).

obtain $\hat{\mathcal{M}}_L \delta \boldsymbol{\Psi} = 0$, where the cumbersome $\hat{\mathcal{M}}_L$ matrix accounts for the inhomogeneous NL DOV profiles, while the 28-dimensional array $\delta \boldsymbol{\Psi}$ contains the site-dependent perturbation amplitudes $\delta \Psi_{\pm}^{j}(w)$ and $\delta \Psi_{0\pm}^{j}(w)$. By calculating numerically the eigenvalues of $\hat{\mathcal{M}}_L$, we obtain the instability gain spectrum $g(l)$ of every NL DOV, depending on the total power P. In Fig. 5(a) we depict the dependence of the maximum gain coefficient Re(g) on the total power P of several NL DOVs with distinct TCs $m = 0, 1, 2$ and fixed perturbation winding number $l = 2\pi/6$. The solid (dashed) lines indicate results corresponding to cored (coreless) MCFs. We find that all NL DOVs are unstable except the nonspinning $m = 0$ NL DOV within a narrow stability window [see Fig. 5(a) and its inset] where Re(g) vanishes. We confirm such semianalytical predictions by direct numerical solutions of Eqs. (1) and (2) by a fourth-order Runge-Kutta algorithm propagating perturbed NL DOVs of both cored and coreless MCFs at the input [see

Figs. 5(b)–5(i)]. Note that only type-④ NL DOVs in cored MCFs with total power $\bar{P} \simeq 0.99$ MW remain stable upon perturbation [see Fig. 5(e)], while other NL DOVs are unstable for both cored and coreless MCFs. We emphasize that the power range centered at $\bar{P}$ where stability is achieved depends on the coupling coefficient C and the nonlinear parameter γ. In turn, we can tailor such a stability window by modulating the MCF core size and intercore separation. In particular, we find that $\bar{P}$ and its power range increase with C for fixed γ, i.e., by reducing the intercore separation d while keeping the core radii r_0 fixed. In turn, our analysis enables the identification of the role played by intersite linear coupling and the on-site Kerr nonlinearity, indicating that instability arises from such two competing effects. Overall, instability reduces when power is reduced and $\bar{P}$ increases when the nonlinear coefficient is reduced.

IV. CONCLUSION

We have investigated the existence and stability of vortex-like NL collective excitations in cored and coreless hexagonal MCFs operating in single-mode regime with polarization degeneracy. By modeling propagation dynamics of such NL fields through nonlinearly coupled discrete Schrödinger equations, we found families of homogeneouslike NL vortex fields characterized by a uniform power distribution over peripheral cores. Linear stability analysis of such collective modes upon perturbations revealed that homogeneouslike NL modes are unstable. We further extended our investigation to the existence of inhomogeneous NL waves with embedded vorticity, finding that only one stable nonspinning localized NL mode can become stable in a narrow power range for cored hexagonal MCFs, while radiation NL dynamics remains unstable for coreless MCFs. Our results shed light on self-organization properties into collective excitations in NL MCFs, indicating that self-organization can be exploited to devise innovative MCF-based communication systems. Furthermore, our analysis can find applications in other communication systems; e.g., it can be useful to gain an understanding of self-cleaning and thermalization in multimode fibers.

ACKNOWLEDGMENTS

[1] A. S. Desyatnikov, L. Turner, and Y. S. Kivshar, Optical vortices and vortex solitons, Prog. Opt. **478**, 291 (2005).

[2] L. Hadzievski, A. Maluckov, A. Rubenchik, and S. Turitsyn, Stable optical vortices in nonlinear multicore fibers, Light Sci. Appl. **4**, e314 (2015).

[3] B. Spektor, A. Normatov, and J. Shamir, Singular beam microscopy, Appl. Opt. **47**, A78 (2008).

[4] F. Tamburini, G. Anzolin, G. Umbriaco, A. Bianchini, and C. Barbieri, Overcoming the Rayleigh criterion limit with optical vortices, Phys. Rev. Lett. **97**, 163903 (2006).

[5] Z. Bouchal and R. Celechovský, Mixed vortex states of light as information carriers, New J. Phys. **6**, 131 (2004).

[6] A. Ashkin, J. M. Dziedzic, and T. Yamane, Optical trapping and manipulation of single cells using infrared laser beams, Nature (London) **330**, 769 (1987).

[7] W. H. Wright, G. J. Sonek, and M. W. Berns, Parametric study of the forces on microspheres held by optical tweezers, Appl. Opt. **33**, 1735 (1994).

[8] M. Friese, H. Rubinsztein-Dunlop, J. Gold, P. Hagberg, and D. Hanstorp, Optically driven micromachine elements, Appl. Phys. Lett. **78**, 547 (2001).

[9] B. A. Malomed, Vortex solitons: Old results and new perspectives, Physica D **399**, 108 (2019).

[10] D. Rozas, C. T. Law, and G. Swartzlander, Propagation dynamics of optical vortices, J. Opt. Soc. Am. B **14**, 3054 (1997).

[11] C. N. Alexeyev, A. V. Volyar, and M. A. Yavorsky, Linear azimuthons in circular fiber arrays and optical angular momentum of discrete optical vortices, Phys. Rev. A **80**, 063821 (2009).

[12] L. Allen, M. W. Beijersbergen, R. J. C. Spreeuw, and J. P. Woerdman, Orbital angular momentum of light and the transformation of Laguerre-Gaussian laser modes, Phys. Rev. A **45**, 8185 (1992).

[13] L. Allen, M. J. Padgett, and M. Babiker, IV the orbital angular momentum of light, Prog. Opt. **39**, 291 (1999).

[14] A. Bekshaev, M. Soskin, and M. Vasnetsov, Paraxial light beams with angular momentum, Ukr. J. Phys. **2**, 73 (2005).

[15] Y. Kivshar and G. P. Agrawal, *Optical Solitons: From Fibers to Photonic Crystals* (Elsevier, Amsterdam, 2003).

[16] S. Lopez-Aguayo, A. S. Desyatnikov, and Y. S. Kivshar, Azimuthons in nonlocal nonlinear media, Opt. Express **14**, 7903 (2006).

[17] O. Maor, N. Dror, and B. A. Malomed, Holding spatial solitons in a pumped cavity with the help of nonlinear potentials, Opt. Lett. **38**, 5454 (2013).

[18] Y. V. Kartashov, V. A. Vysloukh, and L. Torner, Ring surface waves in thermal nonlinear media, Opt. Express **15**, 16216 (2007).

[19] Y. Izdebskaya, G. Assanto, and W. Krolikowski, Observation of stable-vector vortex solitons, Opt. Lett. **40**, 4182 (2015).

[20] O. V. Borovkova, V. E. Lobanov, Y. V. Kartashov, and L. Torner, Rotating vortex solitons supported by localized gain, Opt. Lett. **36**, 1936 (2011).

[21] L. Dong, Y. V. Kartashov, L. Torner, and A. Ferrando, Vortex solitons in twisted circular waveguide arrays, Phys. Rev. Lett. **129**, 123903 (2022).

[22] J. Yang and Z. H. Musslimani, Fundamental and vortex solitons in a two-dimensional optical lattice, Opt. Lett. **28**, 2094 (2003).

[23] D. N. Neshev, T. J. Alexander, E. A. Ostrovskaya, Y. S. Kivshar, H. Martin, I. Makasyuk, and Z. Chen, Observation of discrete vortex solitons in optically induced photonic lattices, Phys. Rev. Lett. **92**, 123903 (2004).

[24] B. Zhu, T. F. Taunay, M. F. Yan, J. M. Fini, M. Fishteyn, E. M. Monberg, and F. V. Dimarcello, Seven-core multicore fiber transmissions for passive optical network, Opt. Express **18**, 11117 (2010).

[25] B. Shalaby, V. Kermene, D. Pagnoux, A. Desfarges-Berthelemot, A. Barthélémy, A. Popp, M. Ahmed, A. Voss, and T. Graf, 19-cores Yb-fiber laser with mode selection for improved beam brightness, Appl. Phys. B **100**, 859 (2010).

[26] F. Chan, A. Lau, and H. Tam, Mode coupling dynamics and communication strategies for multi-core fiber systems, Opt. Express **20**, 4548 (2012).

[27] M. A. Mushref, Vortex field propagation in a hexagonal multi-core fiber array, Opt. Photonics J. **4**, 1 (2014).

[28] F. O. Wu, A. U. Hassan, and D. N. Christodoulides, Thermodynamic theory of highly multimoded nonlinear optical systems, Nat. Photon. **13**, 776 (2019).

[29] N. K. Efremidis and D. N. Christodoulides, Fundamental entropic processes in the theory of optical thermodynamics, Phys. Rev. A **103**, 043517 (2021).

[30] N. K. Efremidis and D. N. Christodoulides, Thermodynamic optical pressures in tight-binding nonlinear multimode photonic systems, Commun. Phys. **5**, 286 (2022).

[31] A. Fusaro, J. Garnier, K. Krupa, G. Millot, and A. Picozzi, Dramatic acceleration of wave condensation mediated by disorder in multimode fibers, Phys. Rev. Lett. **122**, 123902 (2019).

[32] N. Berti, K. Baudin, A. Fusaro, G. Millot, A. Picozzi, and J. Garnier, Interplay of thermalization and strong disorder: Wave turbulence theory, numerical simulations, and experiments in multimode optical fibers, Phys. Rev. Lett. **129**, 063901 (2022).

[33] K. Baudin, J. Garnier, A. Fusaro, N. Berti, G. Millot, and A. Picozzi, Weak Langmuir turbulence in disordered multimode optical fibers, Phys. Rev. A **105**, 013528 (2022).

[34] I. S. Chekhovskoy, O. V. Shtyrina, S. Wabnitz, and M. P. Fedoruk, Finding spatiotemporal light bullets in multicore and multimode fibers, Opt. Express **28**, 7817 (2020).

[35] I. S. Chekhovskoy, A. M. Rubenchik, O. V. Shtyrina, M. A. Sorokina, S. Wabnitz, and M. P. Fedoruk, Nonlinear discrete wavefront shaping for spatiotemporal pulse compression with multicore fibers, J. Opt. Soc. Am. B **35**, 2169 (2018).

[36] R. Guenard, K. Krupa, R. Dupiol, M. Fabert, A. Bendahmane, V. Kermene, A. Desfarges-Berthelemot, J. L. Auguste, A. Tonello, A. Barthélémy, G. Millot, S. Wabnitz, and V. Couderc, Kerr self-cleaning of pulsed beam in an ytterbium doped multimode fiber, Opt. Express **25**, 4783 (2017).

[37] T. Hansson, A. Tonello, T. Mansuryan, F. Mangini, M. Zitelli, M. Ferraro, A. Niang, R. Crescenzi, S. Wabnitz, and V. Couderc, Nonlinear beam self-imaging and self-focusing dynamics in a GRIN multimode optical fiber: Theory and experiments, Opt. Express **28**, 24005 (2020).

[38] F. Mangini, M. Gervaziev, M. Ferraro, D. S. Kharenko, M. Zitelli, Y. Sun, V. Couderc, E. V. Podivilov, S. A. Babin, and S. Wabnitz, Statistical mechanics of beam self-cleaning in GRIN multimode optical fibers, Opt. Express **30**, 10850 (2022).

[39] A. Petrov, M. Odnoblyudov, R. Gumenyuk, L. Minyonok, A. Chumachenko, and V. Filippov, Picosecond Yb-doped tapered fiber laser system with 1.26 MW peak power and 200 W average output power, Sci. Rep. **10**, 17781 (2020).

[40] G. Shi, S. Fu, Q. Sheng, J. Li, Q. Fang, H. Liu, A. Chavez-Pirson, N. Peyghambarian, W. Shi, and J. Yao, Megawatt-peak-power picosecond all-fiber-based laser in MOPA using highly Yb^{3+}-doped LMA phosphate fiber, Opt. Commun. **411**, 133 (2018).

[41] L. J. Kong, M. Zhao, S. Lefrancois, D. G. Ouzounov, C. X. Yang, and F. W. Wise, Generation of megawatt peak power picosecond pulses from a divided-pulse fiber amplifier, Opt. Lett. **37**, 253 (2012).

[42] D. Gloge, Weakly guiding fibers, Appl. Opt. **10**, 2252 (1971).

[43] A. W. Snyder, Coupled-mode theory for optical fibers, J. Opt. Soc. Am. **62**, 1267 (1972).

[44] A. Marini, R. Hartley, A. V. Gorbach, and D. V. Skryabin, Surface-induced nonlinearity enhancement in subwavelength rod waveguides, Phys. Rev. A **84**, 063839 (2011).

[45] A. Mecozzi, C. Antonelli, and M. Shtaif, Coupled Manakov equations in multimode fibers with strongly coupled groups of modes, Opt. Express **20**, 23436 (2012).

[46] F. Lederer, G. I. Stegeman, D. N. Christodoulides, G. Assanto, M. Segev, and Y. Silberberg, Discrete vortex solitons in optics, Phys. Rep. **463**, 1 (2008).

[47] A. Marini, S. Longhi, and F. Biancalana, Optical simulation of neutrino oscillations in binary waveguide arrays, Phys. Rev. Lett. **113**, 150401 (2014).

[48] B. Malomed, Two-dimensional solitons in nonlocal media: A brief review, Symmetry **14**, 1565 (2022).